# Ultra-broadband plasmonic absorber based on titanium nanoholes array structure

S. XIONG[1], B. LIU[2], F. CHEN[2,*]
[1]*Yangtze University College of Aits and Science, Jingzhou 434023, China*
[2]*School of Physics and Optoelectronic Engineering, Yangtze University, Jingzhou, 434023, China*

This paper demonstrates an ultra-broadband plasmonic absorber utilizing a titanium nanohole metasurface in the infrared region. Numerical simulations based on the finite-difference time-domain (FDTD) method reveal that the maximum absorption reaches approximately 96.4 %, with a 90 % absorption bandwidth exceeding 1415 nm. The broadband absorption is attributed to the excitation of the hybrid cavity-plasmon mode and gap plasmon coupling between adjacent nanoholes. Additionally, the effects of various metal materials and geometrical configurations on the proposed absorber are systematically investigated. We anticipate that this ultra-broadband absorber holds significant potential for applications in solar cells and infrared plasmonic detection.

(Received February 12, 2025; accepted October 10, 2025)

*Keywords*: Plasmonic resonance, Titanium, Ultra-broadband perfect absorption, Solar cell

## 1. Introduction

Plasmonic absorber (PA), an important branch of optical devices, has attracted much research attention in recent years due to its unique ability to trap light beyond the diffraction limit [1-6]. With this motivation, a lot of plasmonic devices based on plasmonic absorbers have been proposed and investigated, such as plasmonic tunable absorbers [7-15], solar energy harvesting [16], plasmonic sensors [17-18], thermal emission and photodetections [19]. PA has attracted a lots of attention since it can achieve strong absorption for the incident light in the infrared and visible regions [20-21]. There are numerous ways to enhance the absorption of incident light, such as surface plasmon polaritons and magnetic dipolar resonance, localized surface plasmon and FP cavity mode resonance [22-24].

PA can be classified as narrow-band absorption and broadband absorption. In our previous paper [25-27], we investigate narrow-band absorption based on metamaterial, such as hexagonal-nanorods structure, dielectric-grating and Fabry Perot cavity structure, multilayer-graphene strip grating structure. Compared to narrow-band PA, broadband PA is more valuable in applications such as photodetectors, thermal emitters, and photovolatics [28-29]. Over the past few years, many metallic nanostructures with either polarization-insensitive or polarization-sensitive broadband absorption have been investigated theoretically and demonstrated experimentally. For example, in 2018, Xu. P. et al. proposed an ultra-broadband absorber based on a thin metamaterial nanostructure composed of a periodic array of titanium-silica cubes and an aluminum bottom film, the absorber can achieve 90% absorption bandwidth over 712 nm [30]. In 2017, Ye et al. demonstrated a broadband terahertz absorber with near-unity absorption based on a net-shaped periodically sinusoidally-patterned graphene sheet [31]. Cheng et al. reported the design, fabrication, and measurement of a broadband metamaterial absorber, which consist of lossy frequency selective surface and a metallic ground plane separated by a dielectric layer [32]. In order to produce broadband PA, Ti, and Al materials are often used, since their price is much lower than Au and Ag, and the large imaginary part of dielectric function of Ti makes it possess high loss, which is benefit to broadband PA.

In this paper, an ultra-broadband perfect absorber spanning a broad range from 1179 nm to 2417 nm is achieved based on a periodically nanohole metal-dielectric-metal multilayer structure. The ultra-broadband absorption can be attributed to excitation of plasmon resonance coupling and the trapping plasmon resonance in the dielectric cavity, the position of absorption peak, bandwidth, and absorptance can be tuned by changing geometrical sizes such as the length and width of the rectangular-nanohole, period and the thickness of *Ti* layer and dielectric layer. The designed ultra-broadband perfect absorber exhibits polarization independence. The proposed PA not only has a simple structure, low cost, ultra-broad bandwidth, but also can be fabricated with standard film deposition, colloidal crystal template, and electron beam lithography methods. The designed absorber can find potential applications in solar energy, thermal emitters, and other plasmonic devices [33-34].

## 2. Geometry and simulation method

The proposed ultra-broadband absorber is schematically illustrated in Fig. 1 (a), which consist of *Ti* rectangle nanoholes array placed on the surface of dielectric layer ($SiO_2$-$Al_2O_3$) and coated with a *Al* substrate. Fig. 1 (b) is the side view of unit cell of the proposed plasmonic absorber. The geometrical parameters are as follows: The thickness of *Ti* layer, $SiO_2$ layer, $Al_2O_3$ layer and *Al* substrate are $t_1$, $t_2$, $t_3$, $t_4$. The period and size of the rectangle nanoholes are $p$, $a$ and $b$. In the simulation, periodic boundary conditions were applied in the x and y directions to account for the infinite periodicity of the nanohole array. Perfectly matched layers (PML) with 16 layers were implemented in the z direction to absorb outgoing waves and minimize spurious reflections. A plane wave source with x-polarized electric field was employed, covering the wavelength range of 750–3250 nm to match the target infrared spectrum. The source was placed 500 nm above the structure to ensure normal incidence and avoid near-field coupling artifacts. The total simulation area is 1200 nm × 1200 nm, and a uniform mesh with a minimum grid size of 5 nm was adopted near the Ti nanoholes and dielectric interfaces to resolve subwavelength plasmonic effects. Simulations were iterated until energy decay to $1e^{-5}$ of the initial value to ensure steady-state convergence.

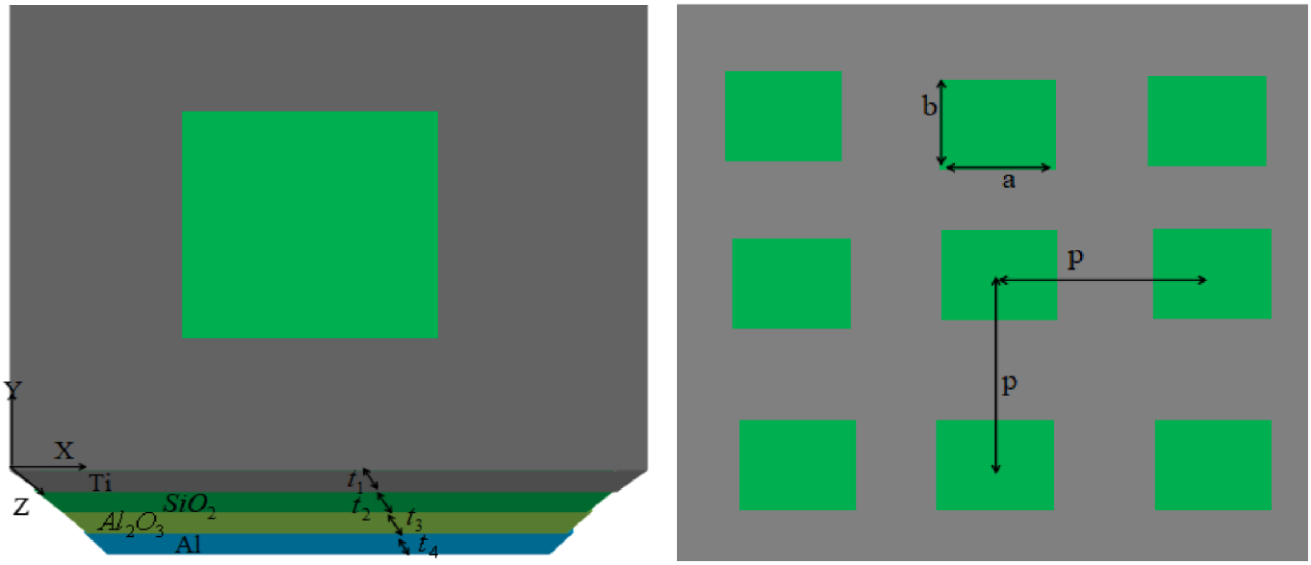


(a) (b)

*Fig. 1. (a) The schematic diagram of the proposed broadband plasmonic absorber composed of multilayer Ti-$SiO_2$-$Al_2O_3$-Al structure. (b) Top view of one unit of the proposed periodic structure (colour online)*

With the transmittance ($T(\lambda)$) and reflectance ($R(\lambda)$) obtained from two 2D frequency-domain power monitors, the absorption ($A(\lambda)$) of the plasmonic absorber can be calculated by the relations: $A(\lambda)=1-T(\lambda)-R(\lambda)$. In the proposed structure, as the 300 nm thick *Al* substrate, the transmittance is almost zero, therefore the absorption $A(\lambda)$ can be represented by $A(\lambda)=1-R(\lambda)$. In the following FDTD simulations, the permittivity of the $SiO_2$ and $Al_2O_3$ is set to 1.45, 1.76, respectively. The frequency-dependent complex permittivity of *Ti*, *Al*, *Ag*, *Ni*, *Au*, *Cu* are taken from Palik [33].

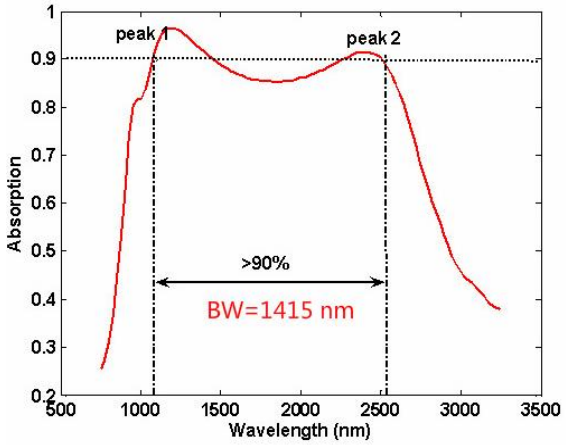


*Fig. 2. The absorption spectrum of the proposed broadband plasmonic absorber calculated by FDTD. (The geometrical parameters were set as $t_1$ = 50 nm, $t_2$ = 120 nm, $t_3$ = 80 nm, $t_4$ = 300 nm, a = 400 nm, b = 400 nm, p = 600 nm (colour online)*

Fig. 2 shows the numerically calculated absorption spectra with $t_1 = 50\ nm$, $t_2 = 120\ nm$, $t_3 = 80\ nm$, $t_4 = 300\ nm$, $a = b = 400\ nm$, $p = 600\ nm$. It can be noticed that the proposed absorber exhibits a high absorption over 90% in a wide wavelength range from 1078 nm to 2493 nm. The 90% bandwidth is about 1415 nm, the average absorption is calculated by $A = \int_{\lambda_2}^{\lambda_1} A(\lambda) d\lambda / (\lambda_1 - \lambda_2)$, where $\lambda_1$ and $\lambda_2$ are 2493 nm and 1078 nm, respectively. The average absorbance over this band is about 92.8 %. And two absorption peaks at 1179 nm and 2417 nm, with corresponding absorbance about 96.4 % and 91.4 %, respectively. Compared to other related plasmonic absorber structures, the bandwidths and absorption efficiency are excellent [36].

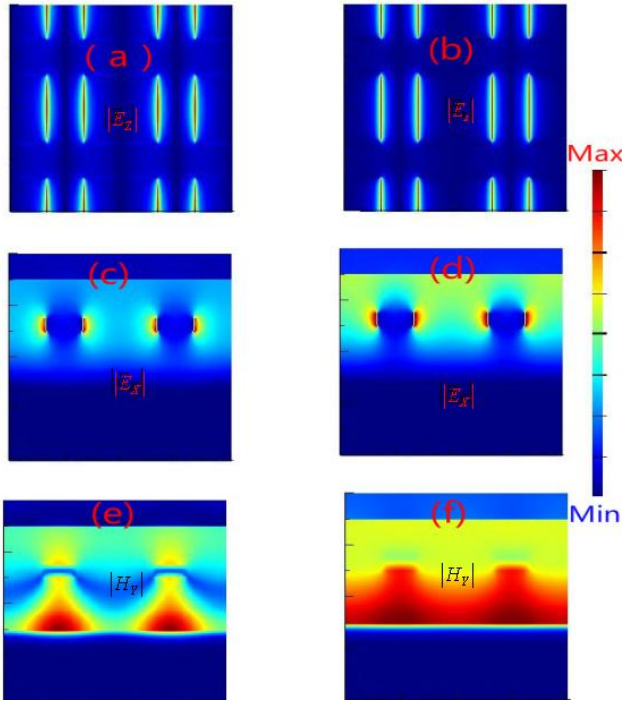


*Fig. 3. (a), (b) Electric field $|E_z|^2$ distribution in the xoy plane at absorption peaks ($\lambda_1 = 1179\ nm$, $\lambda_2 = 2417\ nm$) (c), (d) Electric field, magnetic field $|H_z|^2$ distribution in the xoz plane at absorption peaks ($\lambda_1 = 1179\ nm$, $\lambda_2 = 2417\ nm$) (colour online)*

To investigate the physical mechanism of the ultra-broadband absorption effect, we examined the steady-state electric-field $|E_z|$, $|E_x|$ and magnetic-field $|H_Y|$ distributions of two unit cells. Figs. 3 (a)-(b) shows the electric-field $|E_z|$ distributions of the section $x$ - $y$ plane for two peak wavelengths λ = 1179 nm, 2417 nm. In Fig. 3 (a), at a short wavelength of 1179, most of the electric-field is strongly confined in the rectangular nanoholes, Localized surface plasmon resonance (LSPR) at the Ti nanohole edges (Fig. 3a), confirmed by strong electric field enhancement and dipolar distribution. Figs. 3 (c) and (e) show the steady-state electric - field $|E_x|$ and magnetic – field $|H_Y|$ distributions of the section $x$ - $z$ plane. It can be noticed that plasmon dipolar resonant occurs at the edge of the nanohole. At a long wavelength 2417 nm, from Figs. 3 (b), (d), (f) it can be observed that the strong electric-field is confined in the gap between adjacent nanoholes and the dielectric layer. Since the input electromagnetic wave bounces back between the top *Ti* layer and lower *Al* substrate, just like a Fabry-Perot resonator with low quality factor, the hybrid cavity-plasmon mode formed by Fabry-Pérot (FP) resonance in the $SiO_2/Al_2O_3$ dielectric gap and gap plasmon coupling between adjacent nanoholes makes the absorption bandwidth broaden [37].

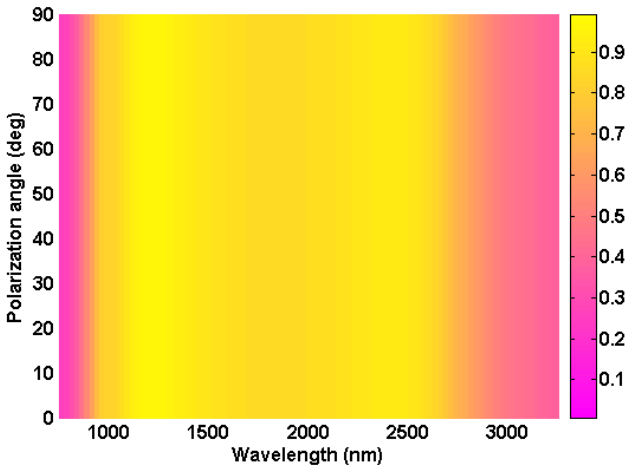


*Fig. 4. The absorption spectra of the broadband plasmonic absorber with different polarization angles (colour online)*

To investigate the influence of polarization angle on the absorption performance of the proposed structure. Fig. 4 shows the evolution of the absorption with the polarization angle of the incident light. It can be observed that when the polarization angle increases from 0 deg to 90 deg, the broadband absorption remains unchanged, This characteristic indicates that the proposed absorber is highly polarization independent. Since the rectangular nanoholes distribution is symmetrical in x and y directions, and the localized plasmonic resonant mode in the nanohole,

the two factors together lead to the polarization-insensitive broadband absorption [38].

To investigate the effect of structural parameters on the absorption spectra. Fig. 5(a) illustrates the evolution of the absorption with the parameter of nanohole *a*, keeping the other structural parameters constant. It can be seen that when *a*<150 nm, the corresponding absorbance is small, this is because a smaller nanohole means a big gap distance and a weaker plasmonic resonance coupling. With increasing $a$ = 150 nm to 400 nm, the absorption bandwidth increases. However, when increasing $a$ from 400 nm to 500 nm, the absorption bandwidth decreases. The absorption spectra with different widths of nanohole $b$ are shown in Fig. 5(b), it can be seen a similar effect, as the increasing of *b*, the bandwidth first increases and then decreases. Therefore, the length and width of the rectangular nanohole in the proposed absorber were selected 400 nm.

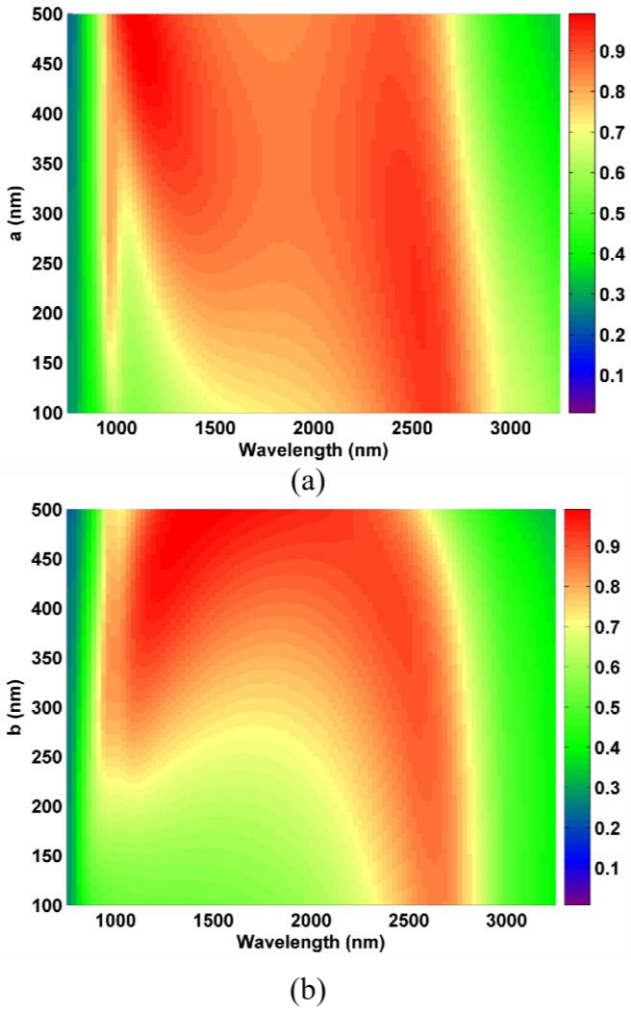


*Fig. 5. The absorption spectra of the broadband plasmonic absorber with different parameters (a) length of air nanohole a . (b) width of air nanohole b (colour online)*

To investigate the thickness of the film on the absorbance of the proposed structure. As shown in Fig. 6 (a), the thickness of *Ti* nanohole is increased from $t_1$=20 nm to 100 nm, the absorption bandwidth increases but the absorbance becomes smaller. It can also be noticed that when $t_1$ < 40 nm, the absorption is mainly located in the high frequency region. Therefore, we can tune the absorption intensity and bandwidth by selecting the thickness of the metal layer. Fig. 6(b) shows the evolution of the absorption with the parameter of dielectric layer thickness $t_2$, it can be seen that when the $t_2$ increases from 80 nm to 160 nm, the absorption band red shifts, and the maximum absorptance moves from the high frequency region to the low frequency region. This phenomenon can be explained by efficient resonant coupling with the incident light by the localized plasmon resonance [39].

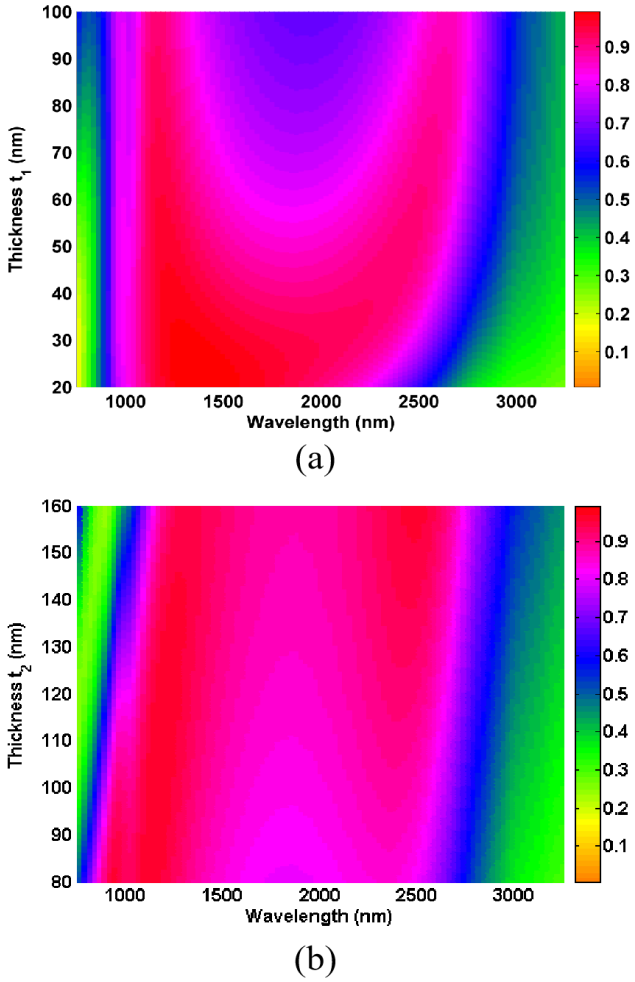


*Fig. 6. The absorption spectra of the broadband plasmonic absorber with different parameters (a) thickness of Ti layer $t_1$. (b) thickness of $SiO_2$ layer $t_2$ (colour online)*

In practical applications, the effects of the material on the absorption performances worth study. Firstly, as shown in Fig. 7 (a), keeping the structural parameters constant,

the top *Ti* metal is replaced by *Ag, Al, Ni*. One can see that when using *Ag* and *Al*, the absorption spectra exhibit narrow resonance in high frequency region. The absorption peak is corresponding plasmonic resonance of *Ag* and *Al*. When the top *Ti* metal is replaced by *Ni*, in high frequency region, the absorption is even higher than *Ti*, but the absorbance is quite low at longer wavelength. When replacing the bottom *Al* layer with *Au, Ag, Cu*. The absorption characteristic is slightly changed. It indicates that the bottom layer is regarded as a back reflector. The proposed ultra-broadband plasmonic absorber holds significant promise for advanced optoelectronic and energy-related applications due to its high absorption efficiency (90% over 1415 nm bandwidth) and cost-effective titanium-based design. Key potential applications include: the broadband absorption spanning 1179–2417 nm (covering near-infrared to short-wavelength infrared) enables high-sensitivity detection in night vision, environmental monitoring, and medical imaging systems. Polarization independence ensures robust performance under arbitrary illumination conditions. With 92.8% average absorptionacross the simulated range, the absorber can enhance solar-thermal conversion efficiency in concentrated solar power (CSP) systems by minimizing reflection losses. Its compatibility with high-temperature stability (via Ti/$Al_2O_3$ layers) suits concentrated solar applications. The use of Ti (instead of Au/Ag) ensures cost scalability and CMOS compatibility [40], while the simple geometry (rectangular nanoholes) facilitates large-area fabrication via nanoimprint lithography or colloidal templating [41]. Further experimental validation could target integration into photovoltaic-thermal (PV-T) hybrid systems or multispectral imaging chips. The fabrication process of the proposed titanium nanoholes array-based absorber involves the following steps: First, a 300 nm-thick aluminum substrate is deposited via standard physical vapor deposition (PVD) techniques [42]. Subsequently, an 80 nm $Al_2O_3$ layer and a 120 nm $SiO_2$ dielectric layer are sequentially deposited using plasma-enhanced chemical vapor deposition (PECVD). A 50 nm titanium film is then sputtered onto the dielectric stack. The rectangular nanoholes array (400 nm × 400 nm dimensions with 600 nm periodicity) is patterned on the titanium layer through a combination of colloidal crystal template self-assembly and reactive ion etching (RIE), or alternatively using electron beam lithography (EBL) for precise nanoscale feature definition. Finally, the structure is completed with optional post-processing steps such as oxygen plasma cleaning to remove residual contaminants. This fabrication approach leverages established nanomanufacturing methods compatible with large-area production while maintaining subwavelength structural precision [43].

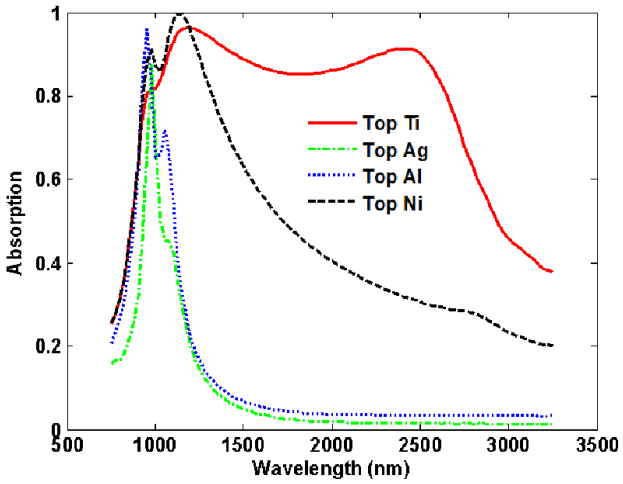


*Fig. 7. The absorption spectra with different top and bottom metals. (a) Top Ti layer replaced by silver (Ag), aluminum (Al) and nickel (Ni). (b) Bottom Al substrate replaced by gold (Au), silver (Ag) and copper (Cu) (colour online)*

## 3. Conclusions

In conclusion, we have proposed an ultra-broadband plasmonic absorber with a nanostructure configured by $Ti - SiO_2 - Al_2O_3$ - Al layer and period rectangular nanohole. Results show that the bandwidth of absorption over 90 % can reach 1415 nm, and the average absorbance over this band is about 92.8 %. The combination of the trapping plasmon resonance in the dielectric cavity and the excitation of plasmon resonance coupling leads to the ultra-broadband absorption. Effect of geometrical sizes, and different metal materials on the absorption performance is studied in detail. Moreover, the proposed ultra-broadband plasmonic absorber exhibits polarization-independence. The designed absorber is not only simple in structure and has high absorption, but also a

big bandwidth. It is believed that these features can pave the ways for solar energy, thermal emitters, and detection in the infrared range.

**Acknowledgments**

**Funding:** Supported by the Yangtze University college students' innovation and entrepreneurship (grantno.z2024323).

## References

[1] S. Xiao, T. Liu, X. Wang, X. Liu, C. Zhou, Physical Review B **102**(8), 085410 (2020).
[2] B. Cai, L. Wu, X. Zhu, Z. Cheng, Y. Cheng, Results in Physics **58**, 107509 (2024).
[3] Wu Ling, Yang Lingling, Cai Bin, Cheng Yongzhi, Cheng Zhengze, Physica B: Condensed Matter **708**, 417205 (2025).
[4] X. Wang, J. Duan, W. Chen, C. Zhou, T. Liu, S. Xiao, Physical Review B **102**(15), 155432 (2020).
[5] Z. Yong, S. Zhang, C. Gong, S. He, Sci. Rep. **6**, 24063 (2016).
[6] Y. Bai, L. Zhao, D. Q. Ju, Y. Y. Jiang, L. H. Liu, Opt. Express **23**(5), 8670 (2015).
[7] L. Li, F. Chen, Physics Letters A **544**, 130489 (2025).
[8] C. Cen, Y. Zhang, C. Liang, X. Chen, Z. Yi, T. Duan, Phys. Lett. A **383**, 3030-5 (2019).
[9] C. Cao, Y. Z. Cheng, Materials **11**(10), 1954 (2018).
[10] Y. Z. Cheng, H. Zhang, X. S. Mao, R. Z. Gong, Materials Letters **219**, 123 (2018).
[11] X. Y. Niu, D. Qi, X. Wang, Y. Z. Cheng, F. Chen, B. W. Li, R. Z. Gong, J. Opt. Soc. Am. A **35**(11), 1832 (2018).
[12] C. Cao, Y. Z. Cheng, Applied Physics A **125**(1), 15 (2019).
[13] Y. Z. Cheng, H. Luo, F. Chen, R. Z. Gong, OSA Continuum **2**(7), 2113 (2019).
[14] Y. Z. Cheng, C. Du, Optical Materials **98**, 109441 (2019).
[15] Y. Z. Cheng, F. Chen, H. Luo, Nanoscale Research Letters **15**(1), 103 (2020).
[16] C. Tang, Z. Yan, Q. Wang, J. Chen, M. Zhu, B. Liu, F. Liu, C. Sui, RCS Adv. **5**, 81866 (2015).
[17] K. Liu, Z. Tu, X. Tang, Z. Li, F. Chen, W. Yang, B. Wang, Plasmonics **19**(3), 1291 (2024).
[18] N. Liu, M. Mesch, T. Weiss, M. Hentschel, H. Giessen, Nano. Lett. **10**, 2342 (2010).
[19] X. L. Liu, T. Talmage, S. Tatiana, F. S. Anthony, M. J. Nan, J. P. Willie, Phys. Rev. Lett. **107**, 045901 (2011).
[20] B. Zhang, Y. Zhao, Q. Hao, B. I. C. Kiraly Khoo, S. Chen, T. J. Huang, Opt. Express **19**, 15211 (2011).
[21] L. Shakiba, M. R. Salehi, F. Emami, Optics Communications **560**, 130498 (2024).
[22] D. Wu, Y. Liu, L. Yu, Z. Yu, L. Chen, R. Ma, H. Ye, Opt. Lett. **42**, 450 (2017).
[23] W. Li, U. Guler, N. Kinsey, G. V. Naik, A. Boltasseva, J. Guan, V. M. Shalaev, A. V. Kildishev, Adv. Mater. **26**, 7959 (2014).
[24] L. Zhou, Y. Zhou, Y. F. Zhu, X. X. Dong, B. L. Gao, Y. Z. Wang, S. Shen, J. Mater. Chem. C **4**, 391 (2016).
[25] F. Chen, D. Z. Yao, H. F. Zhang, L. H. Sun, C. C. Yu, Journal of Electronic Materials **48**, 5603 (2019).
[26] F. Chen, H. F. Zhang, L. H. Sun, J. J. Li, C. C. Yu, Appl. Phys. A **125**, 792 (2019).
[27] L. Zhang, Y. Wang, L. Zhou, F. Chen, Appl. Phys. A **125**, 368 (2019).
[28] Y. Qu, Q. Li, K. Du, L. Cai, J. Lu, M. Qiu, Laser Photonics Rev. **11**, 1700091 (2017).
[29] Y. Qu, Q. Li, L. Cai, M. Pan, P. Ghosh, K. Du, M. Qiu, Light Sci. Appl. **7**, 26 (2018).
[30] L. Lei, S. Li, H. X. Huang, K. Y. Tao, P. Xu, Opt. Express **26**, 5686 (2018).
[31] L. F. Ye, Y. Chen, G. X. Cai, N. Liu, J. F. Zjhu, Z. Y. Song, Q. H. Liu, Opt. Express **25**, 11223 (2017).
[32] L. K. Sun, H. F. Cheng, Y. J. Zhou, J. Wang, Opt. Express **20**, 4675 (2012).
[33] Z. Huang, Y. Zheng, J. Li, Y. Cheng, J. Wang, Z. K. Zhou, L. Chen, Nano Letters **23**(23), 10991 (2023).
[34] M. Deng, S. Kanwal, Z. Wang, C. Cai, Y. Cheng, J. Guan, G. Hu, J. Wang, J. Wen, L. Chen, Nano Letters **24**(46), 14641 (2024).
[35] E. D. Palik, Handbook of Optical Constants of Solids, Academic Press, Orlando, Florida, 1985.
[36] Z. Y. Li, P. Edgar, B. Serkan, K. Hasan, A. Koray, Scientific Reports **5**, 15137 (2015).
[37] F. Le, D. W. Brandl, Y. A. Urzhumov, H. Wang, J. Kundu, N. J. Halas, J. Aizpurua, P. Nordlander. ACS Nano **2**, 707 (2008).
[38] B. X. Zhang, Y. H. Zhao, Q. Z. Hao, B. Kiraly, I. C. Khoo, S. F. Chen, T. J. Huang Opt. Express **19**, 15221 (2011).
[39] J. Chen, Q. Zhang, C. Peng, C. Tang, X. Shen, L. Deng, G. Park, IEEE Photonics Technology Letters **30**, 728 (2018).
[40] L. Zheng, W. Zhou, Z. Ning, G. Wang, X. Cheng, W. Hu, W. Zhou, Z. Liu, S. Yang, K. Xu, M. Luo, Y. Yu, Advanced Optical Materials **6**(23), 1800985 (2018).
[41] M. A. Wood, Journal of the Royal Society Interface **4**(12), 1 (2007).
[42] H. Ichou, N. Arrousse, E. Berdimurodov, N. Aliev, Journal of Bio-and Tribo-Corrosion **10**(1), 3 (2024).
[43] X. You, R. T. Ako, S. Sriram, W. Withayachumnankul, Laser & Photonics Reviews **19**, 2401011 (2025).

*Corresponding author: chenfang@yangtzeu.edu.cn